HHS Public Access

Author manuscript

ACS Appl Bio Mater. Author manuscript; available in PMC 2021 April 26.

Published in final edited form as:

ACS Appl Bio Mater. 2019 August 19; 2(8): 3203–3211. doi:10.1021/acsabm.9b00133.

Thermosensitive Biodegradable Copper Sulfide Nanoparticles for Real-Time Multispectral Optoacoustic Tomography

Sixiang Shi[#1], **Xiaofei Wen**[#1,2,3], **Tingting Li**[1,4], **Xiaoxia Wen**[1], **Qizhen Cao**[1], **Xinli Liu**[5], **Yiyao Liu**[1,4], **Mark D. Pagel**[1], **Chun Li**[1,*]

[1]Department of Cancer Systems Imaging, The University of Texas MD Anderson Cancer Center, Houston, TX 77054, USA

[2]Molecular Imaging Research Center, The Fourth Hospital of Harbin Medical University, Harbin, Heilongjiang 150001, China

[3]Heilongjiang Key Laboratory of Scientific Research in Urology, The Fourth Hospital of Harbin Medical University, Harbin, Heilongjiang 150001, China

[4]Department of Biophysics, University of Electronic Science and Technology of China, Chengdu, Sichuan 610054, China

[5]Department of Pharmacological & Pharmaceutical Sciences, University of Houston, Houston, TX 77204, USA

[#] These authors contributed equally to this work.

Abstract

Although multifunctional inorganic nanoparticles have been extensively explored for effective cancer diagnosis and therapy, their clinical translation has been greatly impeded because of significant uptake in the reticuloendothelial system and concerns about potential toxicity. In this study, we uncovered the thermosensitive biodegradability of CuS nanoparticles, which have classically been considered as stable in bulk state. Polyethylene glycol (PEG)-coated CuS nanoparticles (CuS-PEG) were well preserved at 4 ºC but were rapidly degraded at 37 ºC within 1 week in both *in vitro* and *in vivo* tests. Furthermore, real-time multispectral optoacoustic

[*]**Corresponding Author** Chun Li, PhD Cancer Systems Imaging, The University of Texas MD Anderson Cancer Center, Room 3SCR4.3636, 1881 East Road Unit 1907, Houston, TX 77054, USA. cli@mdanderson.org; Phone: 713-792-5182; Fax: 713-794-5456.

Author Contributions

The manuscript was written through contributions of all authors. All authors have given approval to the final version of the manuscript. S.S. and X.W. conceived, designed and performed the experiments, analyzed the data and wrote the manuscript. T.L., X.W., Q.C. and Y.L. assisted in *in vivo* experiments, including tumor implantation, tail vein injection, and biodistribution studies. X.L. assisted in *in vitro* analysis of the degradation of CuS-PEG nanoparticles. M.D.P. assisted in the experiments of *in vivo* MOST. C.L. conceived the experiment, edited the manuscript and provided overall guidance.

ASSOCIATED CONTENT

Supporting Information

The Supporting Information is available free of charge on the ACS Publications website.

Scheme of the synthesis of CuS-PEG nanoparticles, average hydrodynamic diameters with number, volume, and intensity size distribution, detailed comparison of absorbance profiles when incubated at 4 ºC and 37 ºC under different conditions, detailed comparison of absorbance profiles when incubated for 0, 3, 24, and 168 h under different conditions, photographs of CuS-PEG nanoparticles under different incubation conditions, ICP-OES analysis of mouse feces, *in vivo* PET images, ROI analysis of the blood uptake with nonlinear fitting and *ex vivo* biodistribution studies of intrinsically radiolabeled CuS-PEG nanoparticles, *in situ* tumor MSOT intensity profiles and their nonlinear fitting.

The authors declare no competing financial interest.

tomography, which is more convenient and accurate than traditional ex vivo analysis, was successfully employed to noninvasively demonstrate the biodegradability of CuS-PEG nanoparticles and dynamically monitor their tumor imaging capacity. The temperature-dependent controllable degradation profile and excellent tumor retention of CuS-PEG nanoparticles endows them with great potential for clinical applications since it ensures that the nanoparticles remain intact during production, transportation, and storage but degrade and clear from the body at physiological temperature after accomplishing sufficient diagnosis and therapeutic operations.

Graphical Abstract

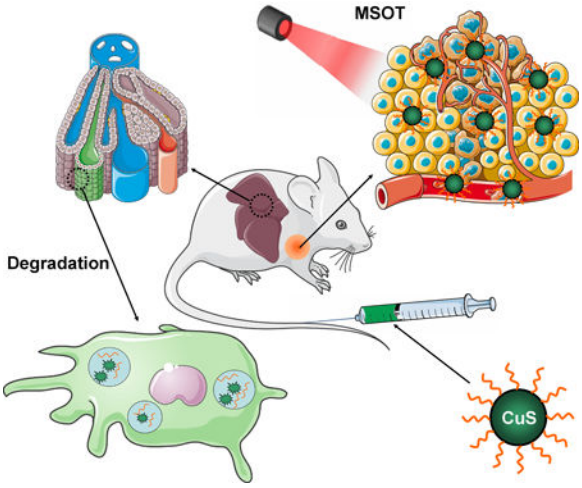

Keywords

copper sulfide; nanoparticles; biodegradable; thermosensitive; multispectral optoacoustic tomography

INTRODUCTION

Nanoparticles have been extensively explored and applied to effective cancer diagnosis and therapy,[1, 2] inspired by the concept of “magic bullet” that selectively attacks pathogens and diseased tissue but leaves healthy cells untouched.[3–5] Multifunctional inorganic nanoparticles based on gold,[6, 7] silicon,[8–11] carbon,[12, 13] and metal oxide and sulfide[14, 15] are some of the most promising candidates due to their unique physical, chemical, and biological properties. However, most inorganic nanoparticles are not degradable and are retained by the reticuloendothelial system (RES), especially the liver, for months to years, or are slowly excreted into bile and feces through the hepatic route over several weeks to months.[16–18] The retained inorganic nanoparticles may trigger oxidative stress and inflammation in the RES,[19–21] leading to concerns about potential long-term toxicity,[22] which significantly impedes the clinical translation of multifunctional inorganic nanoparticles regardless of their tremendous promise and investment in preclinical studies.

Copper sulfide (CuS) nanoparticles have been considered as one of the most promising theranostic nanoplatforms in the past decade.[23, 24] Because of the strong near infrared (NIR)

absorption that is derived from the d–d transition of Cu^{2+} ions, CuS nanoparticles can be employed for photothermal ablation of tumors.[25–27] In addition, the radionuclide copper-64 (^{64}Cu) can be intrinsically incorporated into the nanoparticles during CuS synthesis to permit *in vivo* positron emission tomography (PET) quantification of their retention in tumors.[28, 29] Moreover, CuS nanoparticles can be conjugated with targeting ligands for enhanced tumor retention.[30] In previous studies, CuS was generally considered stable due to its extremely small equilibrium constant (6×10^{-37}) and relatively stable chemical structure that requires high temperature for decomposition.[31, 32] However, the thermodynamic properties change dramatically when the dimensions of CuS decrease to the nanoscale.[32–35] In the study reported herein, we found that CuS nanoparticles degraded almost completely in the mouse liver within 7 days after injection (Figure 1a), which alleviated concerns about potential long-term toxic effects and increase the prospect for their eventual clinical translation.

To date, the assessment of nanoparticle biodegradation has primarily relied on tedious ex vivo analyses that entail tissue harvesting after euthanizing animals at different time intervals after injection. However, these ex vivo analyses are neither convenient nor accurate since degradation can also occur during the post-harvest processing steps. In this study, we successfully utilized real-time multispectral optoacoustic tomography (MSOT) to noninvasively investigate the biodegradation of CuS nanoparticles in the liver and their concomitant accumulation in tumors. In MSOT, the imaging signal is generated by photoacoustic phenomenon in response to the fast absorption transients from CuS-accumulated tissues irradiated by short laser pulses. MSOT is more suitable than PET for exploring *in vivo* degradation since MSOT detects only the signal from intact CuS nanoparticles, rather than degraded Cu ions, whereas PET detects radioactive ^{64}Cu regardless of whether it is present in intact or degraded forms.[13, 36] Thus, MSOT provides an attractive avenue for tracking the degradation kinetics and *in vivo* behavior of amenable nanoparticles in real time and thereby elucidating crucial information for their design, fabrication, and application. In addition, MSOT is multispectral, quantitative and non-radioactive, serving as a promising imaging approach in future clinical setting.[37–41]

RESULTS AND DISCUSSION

CuS nanoparticles were synthesized by a one-step reaction (Figure S1a). In brief, Na_2S was introduced into an aqueous solution of $CuCl_2$ in the presence of PEG-SH and vigorously stirred at 95 ºC for 15 min. The final product, CuS-PEG nanoparticles, were well dispersed with a mean hydrodynamic diameter of 11.1 ± 1.0 nm (number), 25.4 ± 0.9 nm (volume), or 50.8 ± 2.0 nm (intensity) (Figure 1b–d, Figure S1b; n = 3). Successful PEGylation was demonstrated by carbon and oxygen peaks on X-ray photoelectron spectroscopy (XPS) (Figure 1e); PEGylation provided CuS with excellent solubility and biocompatibility for *in vivo* applications. As-synthesized CuS-PEG nanoparticles demonstrated absorbance in the NIR window, peaking at 1050 nm (Figure 1f), which closely matches the emission wavelength of the Nd-YAG laser that has been commonly deployed in medical applications,[42] making it a desirable nanoplatform for simultaneous photoacoustic conversion for MSOT and photothermal conversion for cancer phototherapy.

The degradation of CuS-PEG nanoparticles is temperature dependent. After 7 days, CuS-PEG nanoparticles stored in water at 4 ºC preserved their morphology well with only slight reduction in concentration, whereas those stored at 37 ºC decomposed and were hardly visible on transmission electron microscopy (TEM) (Figure 2a–c). The degradation was further investigated by comparing absorbance intensities at 1050 nm at different temperatures (4 ºC and 37 ºC) and pH values (pH 3, laboratory condition; pH 5, water solution or lysosomal environment; and pH 7.4, physiological environment in blood circulation, extracellular fluid, or cytoplasm in normal tissues). Approximately 95.8 ± 0.8% (pH 3), 96.7 ± 0.6% (pH 5) and 97.5 ± 0.4% (pH 7.4) of CuS-PEG nanoparticles remained intact after 3 h incubation at 4 ºC, and majority (74.5 ± 0.3% at pH 3, 78.8 ± 0.3% at pH 5, and 70.6 ± 0.2% at pH 7.4) remained stable even after incubation for 7 days at 4 ºC (Figure 2d–g, Figure S2, and Figure S3; n = 3). When the temperature increased to 37 ºC, although the majority of CuS-PEG nanoparticles remained stable after incubation for 3 h (91.8 ± 0.9% at pH 3, 96.1 ± 0.4% at pH 5, and 91.4 ± 0.4% at pH 7.4), their stabilities significantly decreased after incubation for 7 days (65.8 ± 0.7% at pH 3, 30.5 ± 0.1% at pH 5, and 17.9 ± 0.1% at pH 7.; Figure 2d–f, and 2h, Figure S2, Figure S3 and Figure S4; n = 3), demonstrating the thermosensitive degradation of CuS-PEG nanoparticles. This degradation profile was additionally confirmed by inductively coupled plasma-optical emission spectrometry (ICP-OES) based on the elemental concentration of Cu (Figure 2i; n = 3). Of note, lower pH exhibited relatively strong protection against the degradation of CuS-PEG nanoparticles (Figure 2h), suggesting that reducing pH can be an alternative way to preserve the nanoparticles when reducing temperature is not applicable.

The mechanism of thermosensitive degradation of CuS-PEG nanoparticles may be primarily attributed to thermal oxidation. Thermal oxidation of larger covellite particles (CuS_{bulk}; > 10 μm) have been performed by heating to higher than 400 ºC.[31, 32] The thermal decomposition of CuS_{bulk} involves several intermediate or final products, including different copper sulfides ($Cu_{1.8}S$ and/or Cu_2S), oxides (Cu_2O and CuO), sulfates (Cu_2SO_4 and $CuSO_4$), and oxysulfates ($CuO{\cdot}CuSO_4$) under different temperatures/conditions.[31, 32] It is well known that the rate of chemical reaction is highly dependent on the particle size.[33–35] However, we surprisingly found that the decomposition temperature could be reduced to as low as the physiological temperature (37 ºC) when the particles were reduced to nanoscale. Given the promising imaging and phototherapeutic applications of CuS nanoparticles, the enhanced thermosensitive degradation profile offers a strong incentive to explore their potential clinical translation by greatly minimizing the concerns about their long-term toxicity. The mechanism of the degradation of CuS-PEG nanoparticles was further validated by XPS, where the majority of sulfur in the nanoparticles retained its S^{2-} configuration under incubation at 4 ºC for 7 days (Figure 2j) but converted to SO_4^{2-} form after incubation in 37 ºC for 7 days (Figure 2k).

CuS-PEG nanoparticles (200 μg) were subsequently injected into healthy nude mice to investigate the *in vivo* degradation property. The majority of intravenously injected nanoparticles are eventually taken up by the RES, especially by the Kupffer cells in the liver, [5] and enter the decomposition or clearance pathway. Therefore, the signals from the liver after injection of CuS-PEG nanoparticles were monitored by MSOT as an index of *in vivo* degradation. Under all the photoacoustic wavelengths acquired in the study, significant liver

uptake was observed after 3 h and 24 h post injection (p.i.) while the liver uptake reduced to near background level after 7 days p.i. (Figure 3a–c; n = 3). Mice were euthanized and livers were harvested at different time points (pre-injection and 3 h, 24 h, and 7 days p.i.) and subjected to ICP-OES to validate the MSOT results (Figure 3d; n = 3). Intrinsic concentration of Cu in the liver, before injection of CuS-PEG nanoparticles, was found to be 4.4 ± 0.4 μg Cu per g of tissue, which corroborated well with the standard Cu concentration in healthy mouse liver.[43] The Cu concentration dramatically increased to 50.0 ± 0.4 μg and 39.9 ± 0.1 μg Cu element in 1 g of liver tissue at 3 h p.i. and 24 h p.i, of CuS-PEG nanoparticles, and significantly decreased to almost background concentrations (8.2 ± 0.4 μg Cu elements per g of liver tissue) after 7 days p.i., confirming the *in vivo* degradation profile of CuS-PEG nanoparticles observed by noninvasive MSOT. Besides the intrinsic oxidation of CuS-PEG, enzymatic degradation may be another reason for the accelerated degradation rate.[44, 45] Clearance of CuS-PEG nanoparticles through hepatic pathway may be also involved in addition to their *in vivo* degradation, as shown by reduced Cu remaining (8.3 ± 0.1 %) in mouse liver compared to *in vitro* results (30.5 ± 0.1 % at pH 5 and 17.9 ± 0.1 % at pH 7.4, Figure 2e–f). The degradation and clearance of CuS nanoparticles was further confirmed by the elevated Cu elemental concentration in feces at different time points after injection of CuS-PEG, as analyzed by ICP-OES (Figure S5; n = 3). In addition to MSOT, dynamic and static PET imaging was performed on [^{64}Cu]CuS-PEG injected healthy mice to validate the biodistribution of CuS nanoparticles (Figure S6a and S6c; n = 4). The blood circulation of [^{64}Cu]CuS-PEG was nonlinearly fitted, achieving a one-phase decay pattern ($y = 24.71e^{-x/72.06} + 0.97$; y represents the blood pool radioactivity (%ID/g); x represents the time after injection (min)) yielding a circulation half-life of 50.0 min (Figure S6b).

Real-time dynamic MSOT was performed after intravenous injection of CuS-PEG nanoparticles (200 μg) into SKOV-3 ovarian tumor-bearing mice to explore their *in vivo* cancer diagnostic capacity. Significant increase in the tumor contrast was observed within the first hour after injection under MSOT wavelengths ranging from 800 nm to 950 nm, suggesting the excellent imaging potential of CuS-PEG nanoparticles (Figure 4; n = 3). Of note, MSOT at 925 nm and 950 nm exhibited the strongest signal from the tumor, corresponding to the absorbance of CuS-PEG which peaks at 1050 nm (Figure 1f). Nonlinear fitting was performed on the basis of real-time dynamic MSOT output to understand the *in vivo* accumulation rate of CuS-PEG nanoparticles in tumor. One-phase exponential association was achieved ($y = y_{max} \cdot (1\text{-}e^{-x/\tau})$; y represents normalized MSOT absorbance intensity (a.u.); x represents the time after injection (min)), showing nearly identical uptake time constant (τ) with different maximal MSOT a.u. (y_{max}) at different wavelengths (Figure S7). By comparing dynamic MSOT signals with the absorbance profile of CuS-PEG nanoparticles, spectral unmixing could be performed *in situ* to visualize the accumulation of CuS-PEG nanoparticles (Figure 4a, green channel), providing a convenient approach to pinpointing extrinsically administered probes from the intrinsic background of tissues. Taken together, these results not only demonstrate a desirable pharmacokinetic profile of CuS-PEG nanoparticles but also confirmed real-time dynamic MSOT as a convenient, efficient, and sensitive modality for cancer diagnosis.

Acute toxicity of CuS-PEG nanoparticles was systematically assessed, since most nanoparticles degraded within 1 week and the degraded Cu^{2+} may generate free radicals

including reactive oxygen species (ROS) and hydroxyl radicals (OH^-) and trigger inflammatory effects.[46] CuS-PEG nanoparticles at the same dose as that for *in vivo* tumor imaging were intravenously injected into healthy C57BL/6 mice. An acceptable elevation of liver enzymes was observed day 1 after injection of CuS-PEG nanoparticles when compared to a control group injected with PBS (aspartate aminotransferase: 2.9 ± 0.6 times; alanine aminotransferase: 1.9 ± 0.6 times; alkaline phosphatase: 0.9 ± 0.1 times; all within the normal range; Figure 5m–o; n = 3), decreasing spontaneously to background levels by day 7 (aspartate aminotransferase: 0.9 ± 0.3 times; alanine aminotransferase: 0.9 ± 0.2 times; alkaline phosphatase: 1.1 ± 0.1 times; Figure 5m–o; n = 3), suggesting negligible, short-term and tolerable hepatic toxicity. In addition, both CuS-PEG and PBS groups exhibited similar hematological results at both day 1 and day 7 and exhibited no significant decrease in body weight, further confirming the safety of CuS-PEG nanoparticles *in vivo* (Figure 5a–l and 5p; n = 3).

CONCLUSION

In conclusion, we reported a thermosensitive biodegradable CuS-PEG nanoplatform that was well preserved at 4 ºC but rapidly degraded at 37 ºC within 1 week. Noninvasive *in vivo* MSOT was performed, successfully visualizing the biodegradation of CuS-PEG nanoparticles and their excellent tumor imaging capacity in real time. MSOT holds great promise for cancer diagnosis and patient profiling, with its ease of operation, low cost, widespread accessibility, and patient compliance. Importantly, the controlled degradation profile of CuS-PEG nanoparticles is of great significance for their translation to clinical settings. Excellent stability at 4 °C promises convenient logistics during production, transportation, and storage, while controllable degradation at 37 °C *in vivo* after accomplishing sufficient diagnosis and therapeutic operations indicates all the qualities of an ideal nanotheranostic agent. Traditional inorganic nanoparticles tend to reside eternally in the liver or clear at an incredibly slow pace, which poses a major obstacle that hinder their clinical applications and bench-to-bedside transition. In contrast, our findings in this study demonstrate that tuning the particles to nanoscale level may dramatically switch many clinically relevant materials from stable bulks to biodegradable nanoparticles, alleviating the potential for long-term toxic effects and advancing closer to clinical translation.

METHODS

Reagents.

Polyethylene glycol (PEG) linkers $mPEG_{5k}$-SH and Chelex 100 resin (50–100 mesh) were purchased from Sigma-Aldrich (St. Louis, MO). Water and all buffers were of Millipore grade and pre-treated with Chelex 100 resin to ensure that the aqueous solution was free of heavy metal. All other chemicals and buffers were obtained from Thermo Fisher Scientific (Fair Lawn, NJ).

Cell lines and animal models.

Human ovarian cancer cells SKOV-3 were obtained from American Type Culture Collection (Manassas, VA) and cultured according to the supplier’s instructions. When they reached

~80% confluence, the cells were harvested for tumor implantation. Six-week-old female nude mice (Taconic Biosciences, Rensselaer, NY) were each subcutaneously injected with 3 × 10^6 SKOV-3 cells in the upper flank to generate the ovarian cancer xenografts. Mice were used for *in vivo* experiments when the tumor diameters reached 6–8 mm. All animal studies were conducted under a protocol approved by The University of Texas MD Anderson Cancer Center.

Synthesis and characterization of CuS-PEG nanoparticles.

CuS-PEG nanoparticles were produced by a straightforward one-step method, modified from our previous reports.[28, 29, 47] Briefly, an aqueous solution of $CuCl_2$ (5 μmol) was added into a 10 mL aqueous solution containing 10 mg of $mPEG_{5k}$-SH and incubated at room temperature under vigorous stirring for 0.5 h. An aqueous solution of Na_2S (10 μmol) was subsequently added into the reaction mixture. The reaction mixture was moved to a 95 ºC oil bath and stirred for 15 min until a dark green solution was obtained, suggesting the completion of CuS-PEG synthesis. The mixture was then transferred to ice-cold water and purified by ultracentrifugation using a 30 kDa MWCO Amicon Ultra-15 centrifugal filter (EMD Millipore, Burlington, MA) for 3 times. To prevent possible aggregation, 1 mg of $mPEG_{5k}$-SH was added into the mixture after each ultracentrifugation step. The final product, CuS-PEG nanoparticles, was stored at 4 °C under nitrogen.

The morphology and size of CuS-PEG nanoparticles were characterized by transmission electron microscopy (TEM; JOEL JEM-1010, JOEL USA, Inc., Peabody, MA). The hydrodynamic size distribution was measured by dynamic light scattering (DLS; Brookhaven Instruments Corporation, Holtsville, NY). Chemical composition was analyzed by X-ray photoelectron spectroscopy (XPS; PHI Quantera II scanning XPS microprobe, Physical Electronics, Chanhassen, MN). The absorbance profile was acquired with a UV-VIS-NIR spectrophotometer (DU 800, Beckman Coulter, Brea, CA). The Cu ion concentration was measured by inductively coupled plasma-optical emission spectrometry (ICP-OES; Agilent 725, Agilent Technologies, Santa Clara, CA).

In vitro degradation of CuS-PEG nanoparticles.

CuS-PEG nanoparticles (0.15 mg mL^{-1}) were incubated in water under different temperatures (4 ºC and 37 ºC) and pH values (pH 3, laboratory condition; pH 5, water solution or lysosomal environment;[48, 49] and pH 7.4, physiological environment in blood circulation, extracellular fluid, and cytoplasm in normal tissues[50]). The morphology, size, and density of CuS-PEG nanoparticles incubated under different test conditions were examined by TEM. Their absorbance profiles were compared based on UV-VIS-NIR analysis as the index of remaining non-degraded CuS-PEG nanoparticles. The remaining nanoparticles were purified by 30 kDa MWCO Amicon Ultra-15 centrifugal filters to remove the degraded CuS and byproducts, followed by thorough digestion in HNO_3 solution (1:1 mixture of remaining CuS-PEG with 70% HNO_3 solution) at 80 ºC for 24 h. The resulting solutions were then diluted with 2% HNO_3 solution and sent for ICP-OES analysis to examine the Cu elemental concentration. Other batches of CuS-PEG nanoparticles after incubation under different conditions were lyophilized and sent for XPS analysis to investigate the changes in chemical composition.

In vivo degradation of CuS-PEG nanoparticles.

CuS-PEG nanoparticles (1 mg mL^{-1}, 200 μL per mouse) were intravenously injected into healthy nude mice. Serial static multispectral optoacoustic tomography (MSOT; iThera Medical, Munich, Germany) was performed to visualize the liver uptake of CuS-PEG nanoparticles at different wavelengths (800 nm, 850 nm, 900 nm, 925 nm, and 950 nm) before injection and at different time points post-injection (p.i.) (3 h, 24 h, and 7 days). The images were reconstructed by linear regression. Region-of-interest (ROI) analyses were performed by comparing the liver signal after normalization (signal intensity at a certain time point – the signal intensity before injection; n = 3). In a separate study, nude mice were intravenously injected with CuS-PEG nanoparticles (1 mg mL^{-1}, 200 μL per mouse) and sacrificed at different time points (before injection and 3 h, 24 h, and 7 days p.i.; n = 3) and their livers and feces were harvested for ICP-OES after complete digestion. The digestion was performed by mixing cryoground liver tissues or feces with 70% HNO_3 solution (1:1 ratio) and incubating at 80 ºC for 48 h. The resulting solutions were then diluted with 2% HNO_3 solution and sent for ICP-OES analysis to examine the Cu elemental concentration.

To confirm the results of MSOT, positron emission tomography (PET) was performed with [^{64}Cu]CuS-PEG nanoparticles. [^{64}Cu]CuS-PEG was synthesized by adding 2 mCi $^{64}CuCl_2$ along with aqueous solution of $CuCl_2$ (5 μmol) into a 10 mL aqueous solution containing 10 mg of $mPEG_{5k}$-SH. The following procedures were exactly the same as the synthesis of non-radioactive CuS-PEG described above. 30 min dynamic scans were performed immediately after i.v. injection of [^{64}Cu]CuS-PEG nanoparticles in the healthy mice, followed by static scans at 3 h p.i. and 24 p.i. (n = 4). After the last scan, the mice were sacrificed and important tissues were collected for *ex vivo* gamma counting studies. Nonlinear fitting was performed to calculate the blood circulation half-life, using one-phase decay ($y = (y_0 - \text{plateau}) \cdot e^{-x/\tau} + \text{plateau}$; y represents the blood pool activity (%ID/g); y_0 represents the blood uptake (%ID/g) immediately after i.v. injection of [^{64}Cu]CuS-PEG; plateau represents the minimum blood uptake (%ID/g); x represents the time after injection (min); τ represents the uptake time constant (min)).

Real-time dynamic MSOT of tumor with CuS-PEG nanoparticles.

CuS-PEG nanoparticles (1 mg mL^{-1}, 200 μL per mouse) were intravenously injected into SKOV-3 tumor-bearing mice. Serial transverse dynamic MSOT was performed to visualize the tumor uptake of CuS-PEG nanoparticles under different wavelengths (800 nm, 850 nm, 900 nm, 925 nm, and 950 nm) for the first hour after injection. The images were reconstructed by linear regression and spectral unmixing. ROI analyses were performed by comparing the tumor signal after normalization (signal intensity at a certain time point – signal intensity before injection; n = 3). Nonlinear fitting was performed based on tumor dynamic MSOT using one-phase exponential association ($y = y_{max} \cdot (1-e^{-x/\tau})$; y represents normalized MSOT absorbance intensity (a.u.); x represents the time after injection (min); τ represents the uptake time constant (min)).

Toxicity assessment of CuS-PEG nanoparticles.

CuS-PEG nanoparticles (1 mg mL^{-1}, 200 μL per mouse) were intravenously injected into 6-week-old healthy female C57BL/6 mice. Body weight and general health were monitored

over 7 days. Blood was drawn at day 1 and day 7 p.i., and a complete blood panel analysis (ADVIA 120 Hematology System, Siemens Healthineers, Erlangen, Germany) and liver chemistry analysis (COBAS INTEGRA 400plus analyzer, Roche Diagnostics, Risch-Rotkreuz, Switzerland) were performed to monitor the changes in hematological and hepatological parameters in response to CuS-PEG administration.

Supplementary Material

Refer to Web version on PubMed Central for supplementary material.

ACKNOWLEDGMENT

We thank S. Goel and S. P. Deming for editing the manuscript. S. Shi was supported by the John S. Dunn, Sr. Distinguished Chair in Diagnostic Imaging. This work was conducted at the MD Anderson Center for Advanced Biomedical Imaging in-part with equipment support from General Electric Healthcare. The Research Animal Support Facility, High Resolution Electron Microscopy Facility, and Small Animal Imaging Facility are supported by a Cancer Center Support Grant from the National Institutes of Health (P30CA016672). X. Wen was supported in part by the China Postdoctoral Science Foundation Grant (2018M641851) and Hei Long Jiang Postdoctoral Foundation (LBH-Z18139).

REFERENCES

(1). Cho K; Wang X; Nie S; Chen ZG; Shin DM Therapeutic nanoparticles for drug delivery in cancer. Clin. Cancer Res 2008, 14, 1310–6. [PubMed: 18316549]

(2). Peer D; Karp JM; Hong S; Farokhzad OC; Margalit R; Langer R. Nanocarriers as an emerging platform for cancer therapy. Nat. Nanotechnol 2007, 2, 751–60. [PubMed: 18654426]

(3). Strebhardt K; Ullrich A. Paul Ehrlich's magic bullet concept: 100 years of progress. Nat. Rev. Cancer 2008, 8, 473–80. [PubMed: 18469827]

(4). Schwartz RS Paul Ehrlich's magic bullets. N. Engl. J. Med 2004, 350, 1079–80. [PubMed: 15014180]

(5). Tsoi KM; MacParland SA; Ma XZ; Spetzler VN; Echeverri J; Ouyang B; Fadel SM; Sykes EA; Goldaracena N; Kaths JM; Conneely JB; Alman BA; Selzner M; Ostrowski MA; Adeyi OA; Zilman A; McGilvray ID; Chan WC Mechanism of hard-nanomaterial clearance by the liver. Nat. Mater 2016, 15, 1212–1221. [PubMed: 27525571]

(6). Dykman L; Khlebtsov N. Gold nanoparticles in biomedical applications: recent advances and perspectives. Chem. Soc. Rev 2012, 41, 2256–82. [PubMed: 22130549]

(7). Boisselier E; Astruc D. Gold nanoparticles in nanomedicine: preparations, imaging, diagnostics, therapies and toxicity. Chem. Soc. Rev 2009, 38, 1759–82. [PubMed: 19587967]

(8). Tang F; Li L; Chen D. Mesoporous silica nanoparticles: synthesis, biocompatibility and drug delivery. Adv. Mater 2012, 24, 1504–34. [PubMed: 22378538]

(9). Chen Y; Chen H; Shi J. In vivo bio-safety evaluations and diagnostic/therapeutic applications of chemically designed mesoporous silica nanoparticles. Adv. Mater 2013, 25, 3144–76. [PubMed: 23681931]

(10). Shi S; Chen F; Cai W. Biomedical applications of functionalized hollow mesoporous silica nanoparticles: focusing on molecular imaging. Nanomedicine (Lond) 2013, 8, 2027–39. [PubMed: 24279491]

(11). Zhang Y; Hsu BY; Ren C; Li X; Wang J. Silica-based nanocapsules: synthesis, structure control and biomedical applications. Chem. Soc. Rev 2015, 44, 315–35. [PubMed: 25310644]

(12). Yang K; Feng L; Shi X; Liu Z. Nano-graphene in biomedicine: theranostic applications. Chem. Soc. Rev 2013, 42, 530–47. [PubMed: 23059655]

(13). Shi S; Xu C; Yang K; Goel S; Valdovinos HF; Luo H; Ehlerding EB; England CG; Cheng L; Chen F; Nickles RJ; Liu Z; Cai W. Chelator-Free Radiolabeling of Nanographene: Breaking the

Stereotype of Chelation. Angew. Chem. Int. Ed. Engl 2017, 56, 2889–2892. [PubMed: 28170126]

(14). Liong M; Lu J; Kovochich M; Xia T; Ruehm SG; Nel AE; Tamanoi F; Zink JI Multifunctional inorganic nanoparticles for imaging, targeting, and drug delivery. ACS Nano 2008, 2, 889–96. [PubMed: 19206485]

(15). Chandra S; Barick KC; Bahadur D. Oxide and hybrid nanostructures for therapeutic applications. Adv. Drug Deliv. Rev 2011, 63, 1267–81. [PubMed: 21729727]

(16). Yu M; Zheng J. Clearance Pathways and Tumor Targeting of Imaging Nanoparticles. ACS Nano 2015, 9, 6655–74. [PubMed: 26149184]

(17). Zhang YN; Poon W; Tavares AJ; McGilvray ID; Chan WCW Nanoparticle-liver interactions: Cellular uptake and hepatobiliary elimination. J. Control Release 2016, 240, 332–348. [PubMed: 26774224]

(18). Longmire M; Choyke PL; Kobayashi H. Clearance properties of nano-sized particles and molecules as imaging agents: considerations and caveats. Nanomedicine (Lond) 2008, 3, 703–17. [PubMed: 18817471]

(19). Nel A; Xia T; Madler L; Li N. Toxic potential of materials at the nanolevel. Science 2006, 311, 622–7. [PubMed: 16456071]

(20). Khanna P; Ong C; Bay BH; Baeg GH Nanotoxicity: An Interplay of Oxidative Stress, Inflammation and Cell Death. Nanomaterials (Basel) 2015, 5, 1163–1180. [PubMed: 28347058]

(21). Xia T; Kovochich M; Brant J; Hotze M; Sempf J; Oberley T; Sioutas C; Yeh JI; Wiesner MR; Nel AE Comparison of the abilities of ambient and manufactured nanoparticles to induce cellular toxicity according to an oxidative stress paradigm. Nano Lett. 2006, 6, 1794–807. [PubMed: 16895376]

(22). Sharifi S; Behzadi S; Laurent S; Forrest ML; Stroeve P; Mahmoudi M. Toxicity of nanomaterials. Chem. Soc. Rev 2012, 41, 2323–43. [PubMed: 22170510]

(23). Goel S; Chen F; Cai W. Synthesis and biomedical applications of copper sulfide nanoparticles: from sensors to theranostics. Small 2014, 10, 631–45. [PubMed: 24106015]

(24). Zhou M; Tian M; Li C. Copper-Based Nanomaterials for Cancer Imaging and Therapy. Bioconjug. Chem 2016, 27, 1188–99. [PubMed: 27094828]

(25). Dong K; Liu Z; Li Z; Ren J; Qu X. Hydrophobic anticancer drug delivery by a 980 nm laser-driven photothermal vehicle for efficient synergistic therapy of cancer cells in vivo. Adv. Mater 2013, 25, 4452–8. [PubMed: 23798450]

(26). Goel S; Ferreira CA; Chen F; Ellison PA; Siamof CM; Barnhart TE; Cai W. Activatable Hybrid Nanotheranostics for Tetramodal Imaging and Synergistic Photothermal/Photodynamic Therapy. Adv. Mater 2018, 30.

(27). Tian Q; Tang M; Sun Y; Zou R; Chen Z; Zhu M; Yang S; Wang J; Hu J. Hydrophilic flower-like CuS superstructures as an efficient 980 nm laser-driven photothermal agent for ablation of cancer cells. Adv. Mater 2011, 23, 3542–7. [PubMed: 21735487]

(28). Zhou M; Zhang R; Huang M; Lu W; Song S; Melancon MP; Tian M; Liang D; Li C. A chelator-free multifunctional [64Cu]CuS nanoparticle platform for simultaneous micro-PET/CT imaging and photothermal ablation therapy. J. Am. Chem. Soc 2010, 132, 15351–8. [PubMed: 20942456]

(29). Zhou M; Chen Y; Adachi M; Wen X; Erwin B; Mawlawi O; Lai SY; Li C. Single agent nanoparticle for radiotherapy and radio-photothermal therapy in anaplastic thyroid cancer. Biomaterials 2015, 57, 41–9. [PubMed: 25913249]

(30). Zhou M; Song S; Zhao J; Tian M; Li C. Theranostic CuS Nanoparticles Targeting Folate Receptors for PET Image-Guided Photothermal Therapy. J. Mater. Chem. B 2015, 3, 8939–8948. [PubMed: 27725882]

(31). Dunn JG; Muzenda C. Thermal oxidation of covellite (CuS). Thermochim. Acta 2001, 369, 117–123.

(32). Simonescu CM; Teodorescu VS; Carp O; Patron L; Capatina C. Thermalbehaviour of CuS (covellite) obtained from copper–thiosulfate system. J. Therm. Anal. Calorim 2007, 88, 71–76.

(33). Li W; Xue Y; Cui Z. Size dependence of surface thermodynamic properties of nanoparticles and its determination method by reaction rate constant. Physica B Condens. Matter 2016, 495, 98–105.

(34). Fu Q; Cui Z; Xue Y; Duan H. Research of Size- and Shape-Dependent Thermodynamic Properties of the Actual Melting Process of Nanoparticles. J. Phys. Chem. C 2018, 122, 15713–15722.

(35). Xiong S; Qi W; Cheng Y; Huang B; Wang M; Li Y. Universal relation for size dependent thermodynamic properties of metallic nanoparticles. Phys. Chem. Chem. Phys 2011, 13, 10652–60. [PubMed: 21523307]

(36). Zhang Y; Jeon M; Rich LJ; Hong H; Geng J; Shi S; Barnhart TE; Alexandridis P; Huizinga JD; Seshadri M; Cai W; Kim C; Lovell JF Non-invasive multimodal functional imaging of the intestine with frozen micellar naphthalocyanines. Nat. Nanotechnol 2014, 9, 631–8. [PubMed: 24997526]

(37). Wang LV; Yao J. A practical guide to photoacoustic tomography in the life sciences. Nat. Methods 2016, 13, 627–38. [PubMed: 27467726]

(38). Wang X; Pang Y; Ku G; Xie X; Stoica G; Wang LV Noninvasive laser-induced photoacoustic tomography for structural and functional in vivo imaging of the brain. Nat. Biotechnol 2003, 21, 803–6. [PubMed: 12808463]

(39). Razansky D; Distel M; Vinegoni C; Ma R; Perrimon N; Köster RW; Ntziachristos V. Multispectral opto-acoustic tomography of deep-seated fluorescent proteins in vivo. Nat. Photonics 2009, 3, 412–417.

(40). Foroutan F; Jokerst JV; Gambhir SS; Vermesh O; Kim HW; Knowles JC Sol-gel synthesis and electrospraying of biodegradable (P2O5)55-(CaO)30-(Na2O)15 glass nanospheres as a transient contrast agent for ultrasound stem cell imaging. ACS Nano 2015, 9, 1868–1877. [PubMed: 25625373]

(41). Kim T; Lemaster JE; Chen F; Li J; Jokerst JV Photoacoustic Imaging of Human Mesenchymal Stem Cells Labeled with Prussian Blue-Poly(l-lysine) Nanocomplexes. ACS Nano 2017, 11, 9022–9032. [PubMed: 28759195]

(42). Beer M; Jocham D; Beer A; Staehler G. Adjuvant laser treatment of bladder cancer: 8 years' experience with the Nd-YAG laser 1064 nm. Br. J. Urol 1989, 63, 476–8. [PubMed: 2731006]

(43). Keen CL; Hurley LS Developmental changes in concentrations of iron, copper, and zinc in mouse tissues. Mech. Ageing. Dev 1980, 13, 161–76. [PubMed: 7432004]

(44). Lovell JF; Jin CS; Huynh E; Jin H; Kim C; Rubinstein JL; Chan WC; Cao W; Wang LV; Zheng G. Porphysome nanovesicles generated by porphyrin bilayers for use as multimodal biophotonic contrast agents. Nat. Mater 2011, 10, 324–32. [PubMed: 21423187]

(45). Chen M; Zeng G; Xu P; Lai C; Tang L. How Do Enzymes 'Meet' Nanoparticles and Nanomaterials? Trends Biochem. Sci 2017, 42, 914–930. [PubMed: 28917970]

(46). Simpson JA; Cheeseman KH; Smith SE; Dean RT Free-radical generation by copper ions and hydrogen peroxide. Stimulation by Hepes buffer. Biochem. J 1988, 254, 519–23. [PubMed: 3178771]

(47). Ku G; Zhou M; Song S; Huang Q; Hazle J; Li C. Copper sulfide nanoparticles as a new class of photoacoustic contrast agent for deep tissue imaging at 1064 nm. ACS Nano 2012, 6, 7489–96. [PubMed: 22812694]

(48). Mindell JA Lysosomal acidification mechanisms. Annu. Rev. Physiol 2012, 74, 69–86. [PubMed: 22335796]

(49). Grossi M; Morgunova M; Cheung S; Scholz D; Conroy E; Terrile M; Panarella A; Simpson JC; Gallagher WM; O'Shea DF Lysosome triggered near-infrared fluorescence imaging of cellular trafficking processes in real time. Nat. Commun 2016, 7, 10855. [PubMed: 26927507]

(50). Roos A; Boron WF Intracellular pH. Physiol. Rev 1981, 61, 296–434. [PubMed: 7012859]

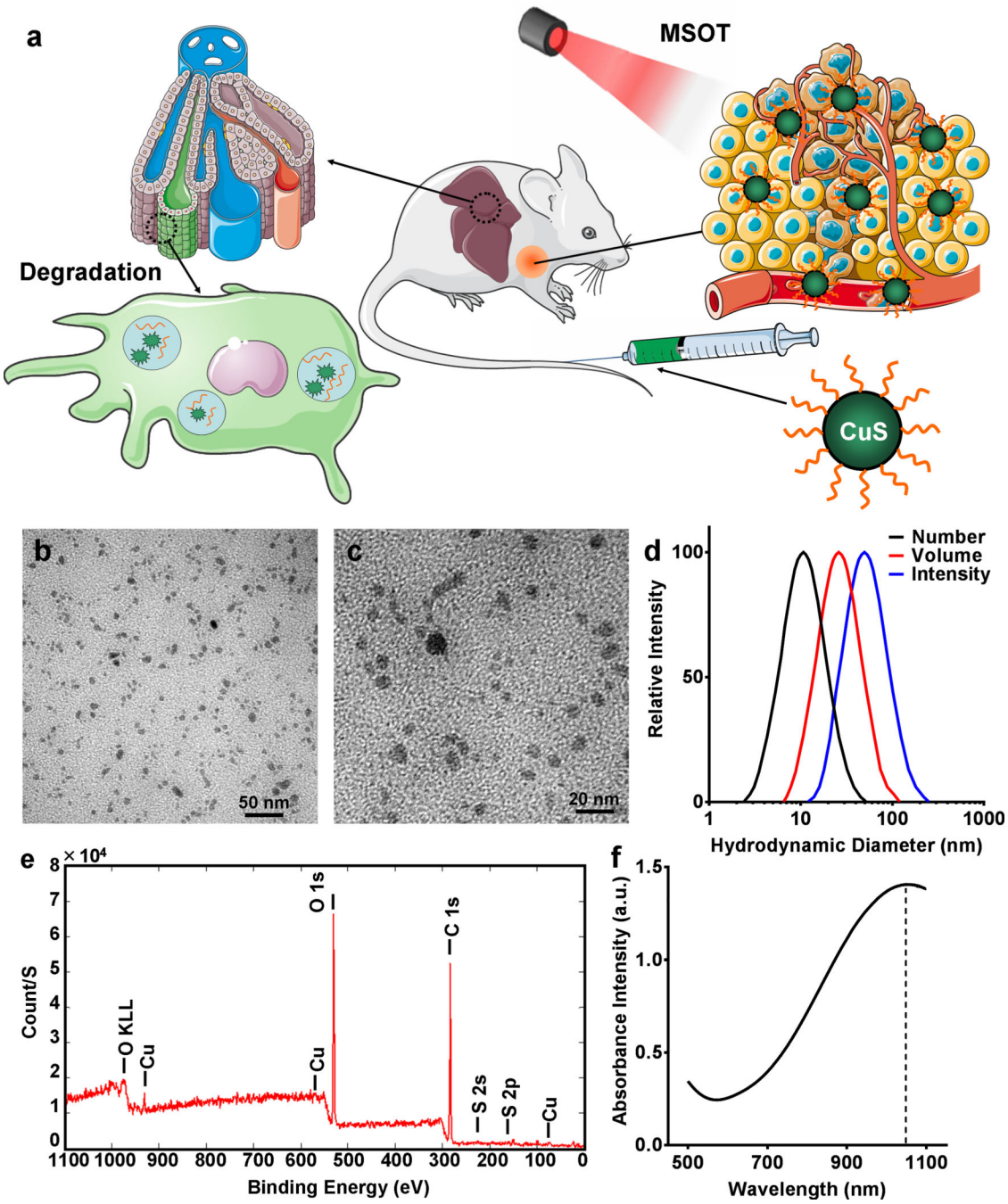

Figure 1.

Scheme and characterization of biodegradable CuS-PEG nanoparticles. (**a**) Schematic illustration of CuS-PEG nanoparticles that allow MSOT-based tumor detection and degradation in the liver within 7 days. The scheme was modified from Servier Medical Art (http://smart.servier.com/), licensed under a Creative Commons Attribution 3.0 Generic License. Nanoparticle size was measured by TEM at magnification of 300k (**b**) and 500k (**c**) and dynamic light scattering (DLS) based on number, volume, and intensity distributions

(**d**). (**e**) Chemical composition of CuS-PEG nanoparticles was characterized by XPS. (**f**) Absorbance profile was characterized by UV-VIS-NIR spectrometry.

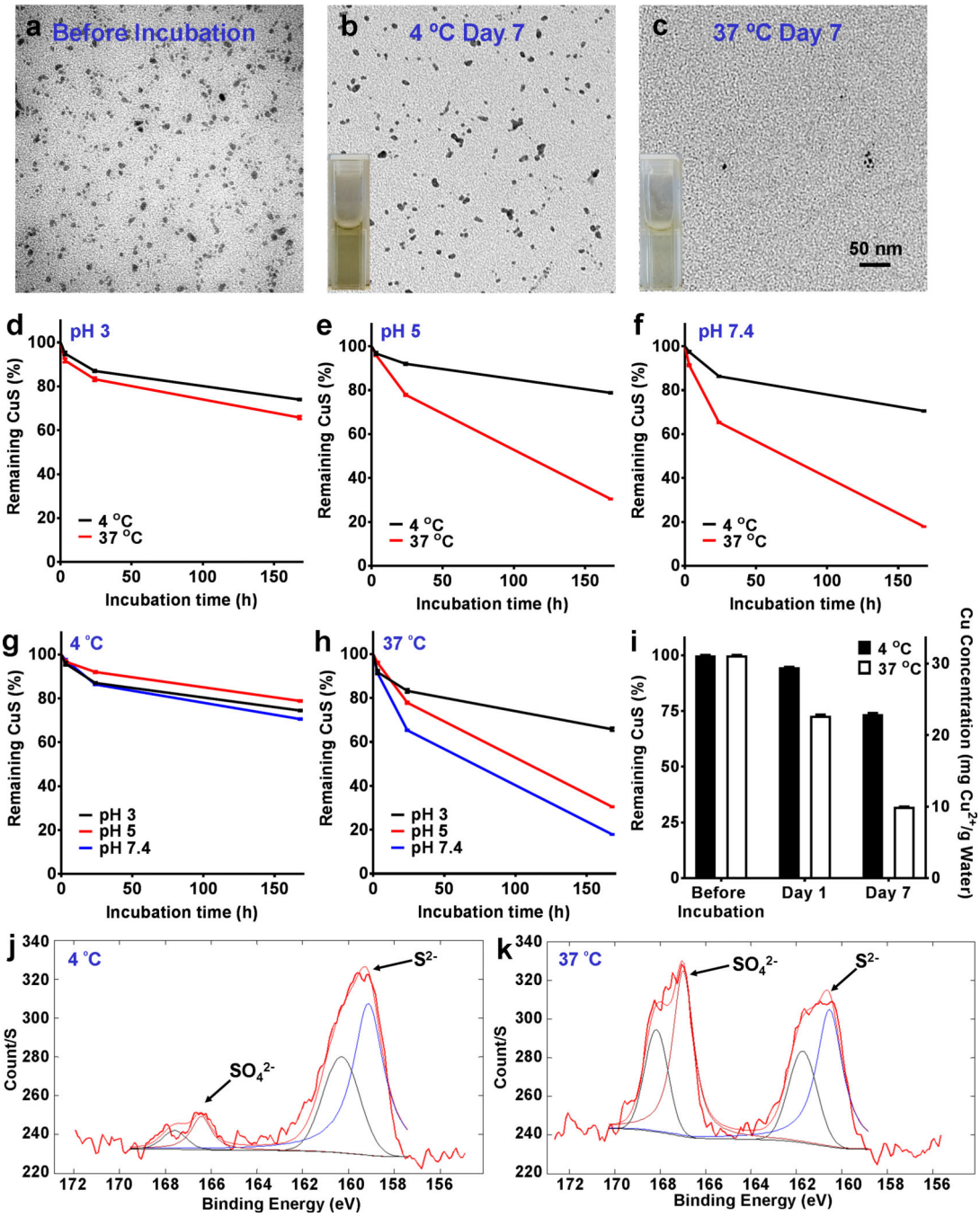

Figure 2.

In vitro degradation of CuS-PEG nanoparticles. TEM images show CuS-PEG nanoparticles before incubation (**a**) and after 7-day incubation in water (pH 5) at 4 ºC (**b**) and 37 ºC (**c**). Thermosensitive degradation profiles were compared over 7-day incubation at pH 3 (**d**), pH 5 (**e**), and pH 7.4 (**f**) or at 4 ºC (**g**) and 37 ºC (**h**) (n = 3). (**i**) Thermosensitive degradation was confirmed by ICP-OES, which showed significantly different Cu concentrations in the retained CuS-PEG nanoparticles between the 4 ºC and 37 ºC groups, after ultracentrifugation

with 30,000 kDa filter (n = 3). The degradation mechanism was validated by XPS of CuS-PEG nanoparticles after 7-day incubation in water (pH 5) at 4 ºC (**j**) and 37 ºC (**k**).

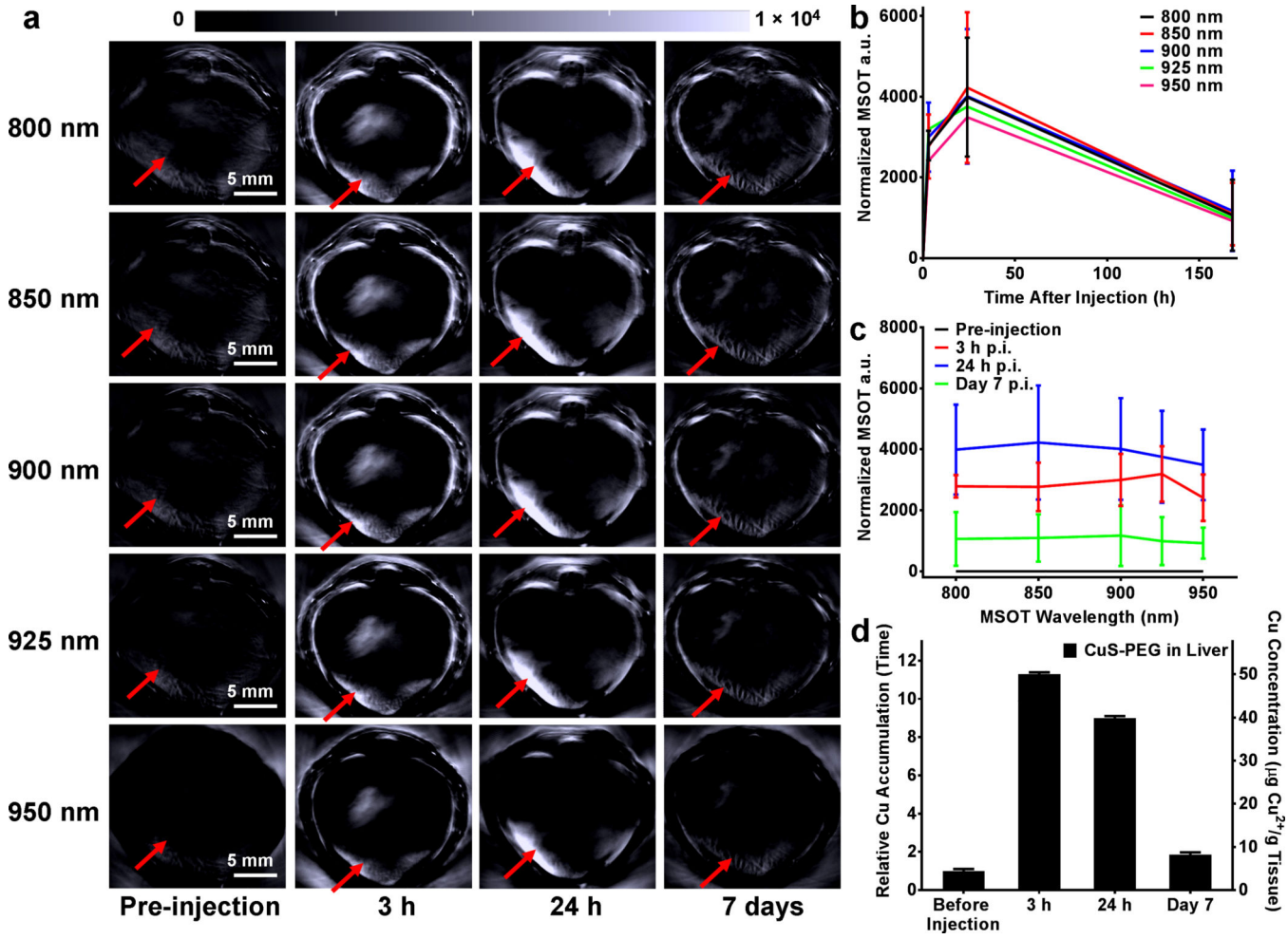

Figure 3.

In vivo degradation and MSOT of CuS-PEG nanoparticles in the liver. (**a**) Serial static transverse MSOT images were obtained under different wavelengths before intravenous injection and at different time points after intravenous injection of nanoparticles. The red arrows indicate the location of the liver. Region-of-interest (ROI) analyses were performed by comparing the liver signal after normalization (signal intensity at a certain time point – signal intensity before injection) at different wavelengths (**b**) and at different time points (**c**) (n = 3). (**d**) The MSOT results were validated by ICP-OES, which showed a decrease in Cu concentration in the liver (n = 3).

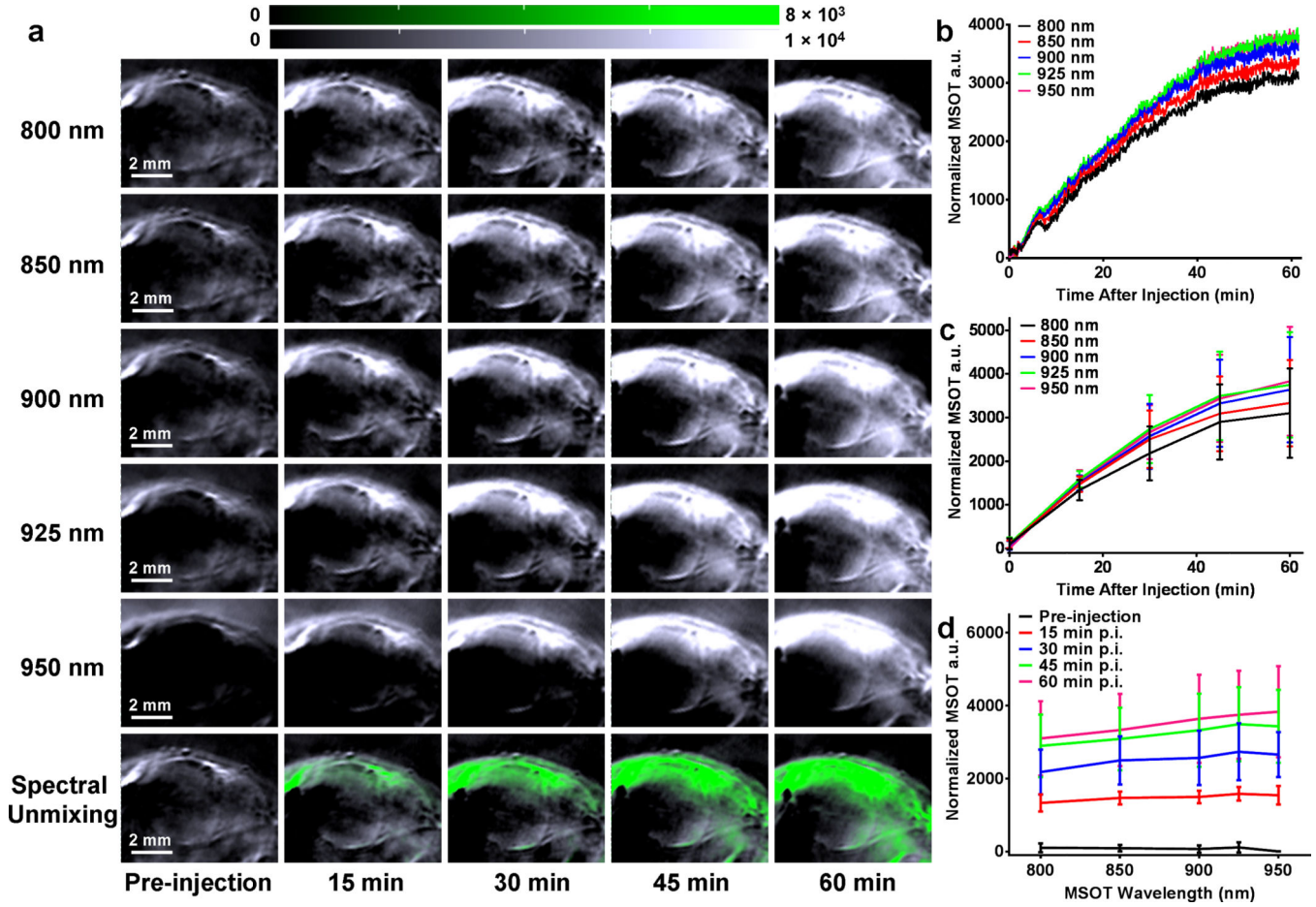

Figure 4.

Real-time dynamic MSOT of tumor with CuS-PEG nanoparticles. (**a**) Serial transverse dynamic MSOT images of SKOV-3 tumor under different wavelengths at different time points after intravenous injection of CuS-PEG nanoparticles. White channel indicates the MSOT intensity. Green channel indicates the distribution of CuS-PEG nanoparticles after spectral unmixing. (**b**) *In situ* tumor MSOT intensity was acquired for the first hour after injection of CuS-PEG nanoparticles. Average tumor MSOT intensity was analyzed by comparing the tumor signals after normalization (signal intensity at a certain time point – the signal intensity before injection) at different wavelengths (**c**) and time points (**d**) (n = 3).

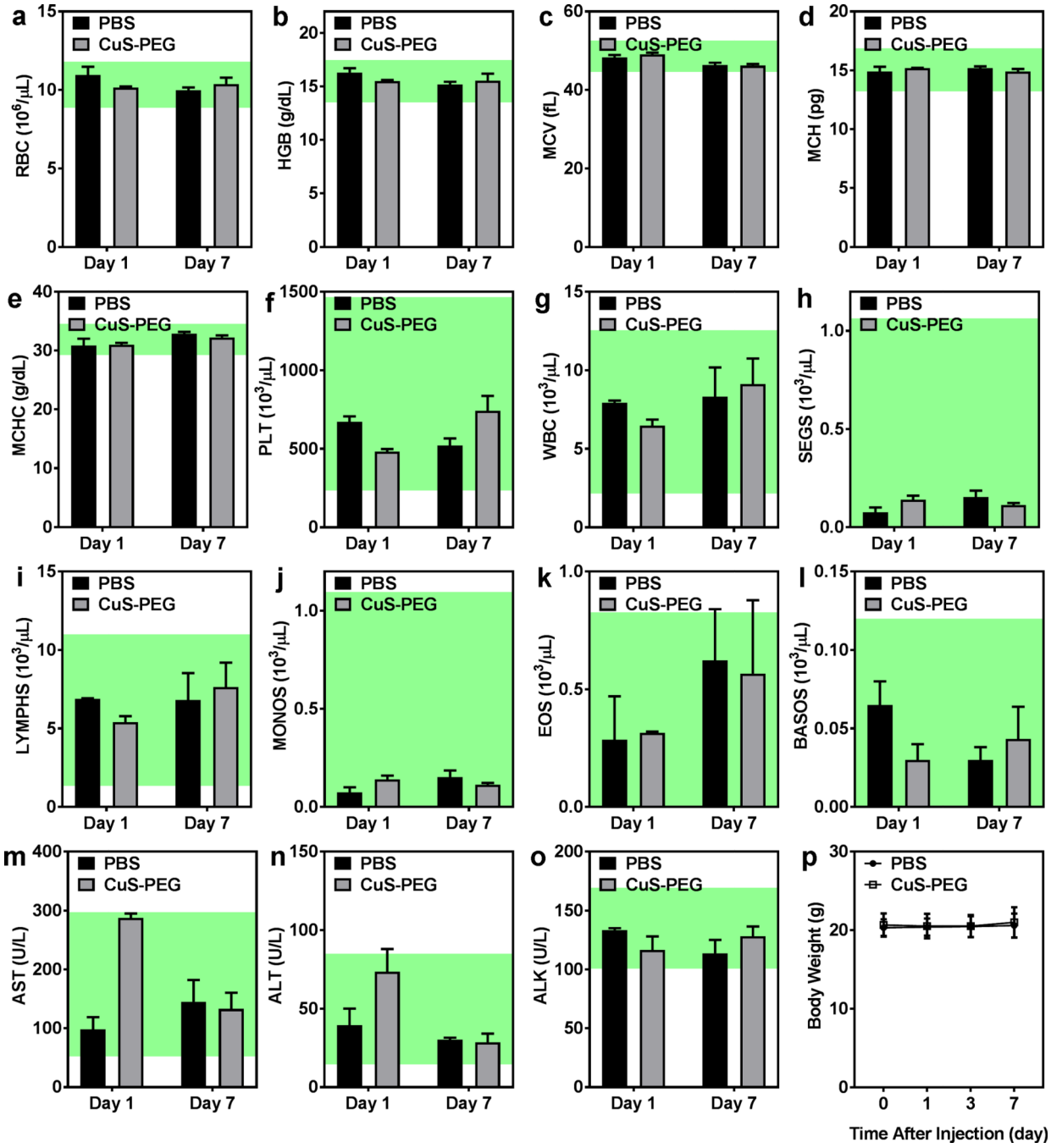

Figure 5.

Short-term toxicity of CuS-PEG nanoparticles was investigated via complete hematology assay, including red blood cell count (**a**), hemoglobin concentration (**b**), mean corpuscular volume (**c**), mean corpuscular hemoglobin (**d**), mean corpuscular hemoglobin concentration (**e**), platelet count (**f**), white blood cell count (**g**), segmented neutrophil count (**h**), lymphocyte count (**i**), monocyte count (**j**), eosinophil count (**k**), and basophil count (**l**), liver chemistry analysis, including concentrations of aspartate aminotransferase (**m**), alanine aminotransferase (**n**) and alkaline phosphatase (**o**), and the body weight (**p**) (n = 3). The

shaded regions represent normal ranges of hematology and liver chemistry parameters in female C57BL/6 mice provided by Taconic Biosciences.